

Nanoscale cathodoluminescence spectroscopy probing the nitride quantum wells in an electron microscope

Zhetong Liu(刘哲彤), Bingyao Liu(刘秉尧), Dongdong Liang(梁冬冬), Xiaomei Li(李晓梅), Xiaomin Li(李晓敏), Li Chen(陈莉), Rui Zhu(朱瑞), Jun Xu(徐军), Tongbo Wei(魏同波), Xuedong Bai(白雪冬), and Peng Gao(高鹏)
Citation: Chin. Phys. B, 2024, 33 (**3**): 038502. DOI: 10.1088/1674-1056/ad1c56
Journal homepage: http://cpb.iphy.ac.cn; http://iopscience.iop.org/cpb

What follows is a list of articles you may be interested in

Investigation of degradation and recovery characteristics of NBTI in 28-nm high-*k* metal gate process

Wei-Tai Gong(巩伟泰), Yan Li(李闫), Ya-Bin Sun(孙亚宾), Yan-Ling Shi(石艳玲), and Xiao-Jin Li(李小进)
Chin. Phys. B, 2023, 32 (**12**): 128502. DOI: 10.1088/1674-1056/ace034

Proton induced radiation effect of SiC MOSFET under different bias

Hong Zhang(张鸿), Hong-Xia Guo(郭红霞), Zhi-Feng Lei(雷志锋), Chao Peng(彭超), Wu-Ying Ma(马武英), Di Wang(王迪), Chang-Hao Sun(孙常皓), Feng-Qi Zhang(张凤祁), Zhan-Gang Zhang(张战刚), Ye Yang(杨业), Wei Lv(吕伟), Zhong-Ming Wang(王忠明), Xiang-Li Zhong(钟向丽), and Xiao-Ping Ouyang(欧阳晓平)
Chin. Phys. B, 2023, 32 (**10**): 108503. DOI: 10.1088/1674-1056/acbe31

A polarization mismatched p-GaN/p-$Al_{0.25}Ga_{0.75}N$/p-GaN structure to improve the hole injection for GaN based micro-LED with secondary etched mesa

Yidan Zhang(张一丹), Chunshuang Chu(楚春双), Sheng Hang(杭升), Yonghui Zhang(张勇辉),Quan Zheng(郑权), Qing Li(李青), Wengang Bi(毕文刚), and Zihui Zhang(张紫辉)
Chin. Phys. B, 2023, 32 (**1**): 018509. DOI: 10.1088/1674-1056/ac9b35

Dynamic modeling of total ionizing dose-induced threshold voltage shifts in MOS devices

Guangbao Lu(陆广宝), Jun Liu(刘俊), Chuanguo Zhang(张传国), Yang Gao(高扬), and Yonggang Li(李永钢)
Chin. Phys. B, 2023, 32 (**1**): 018506. DOI: 10.1088/1674-1056/ac9fc4

Graphene-based heterojunction for enhanced photodetectors

Haiting Yao(姚海婷), Xin Guo(郭鑫), Aida Bao(鲍爱达), Haiyang Mao(毛海央),Youchun Ma(马游春), and Xuechao Li(李学超)
Chin. Phys. B, 2022, 31 (**3**): 038501. DOI: 10.1088/1674-1056/ac1b8b

---

RAPID COMMUNICATION

Nanoscale cathodoluminescence spectroscopy probing the nitride quantum wells in an electron microscope

Zhetong Liu(刘哲彤)[1,2], Bingyao Liu(刘秉尧)[1,2], Dongdong Liang(梁冬冬)[3,4], Xiaomei Li(李晓梅)[1], Xiaomin Li(李晓敏)[5], Li Chen(陈莉)[1], Rui Zhu(朱瑞)[1,†], Jun Xu(徐军)[1], Tongbo Wei(魏同波)[3,4,‡], Xuedong Bai(白雪冬)[5,§], and Peng Gao(高鹏)[1,2,6,¶]

[1] *Electron Microscopy Laboratory, School of Physics, Peking University, Beijing* 100871, *China*
[2] *Academy for Advanced Interdisciplinary Studies, Peking University, Beijing* 100871, *China*
[3] *Research and Development Center for Semiconductor Lighting Technology, Institute of Semiconductors, Chinese Academy of Sciences, Beijing* 100083, *China*
[4] *Center of Materials Science and Optoelectronics Engineering, University of Chinese Academy of Sciences, Beijing* 100049, *China*
[5] *Beijing National Laboratory for Condensed Matter Physics, Institute of Physics, Chinese Academy of Sciences, Beijing* 100190, *China*
[6] *International Center for Quantum Materials, Peking University, Beijing* 100871, *China*

(Received 29 August 2023; revised manuscript received 14 December 2023; accepted manuscript online 9 January 2024)

To gain further understanding of the luminescence properties of multiquantum wells and the factors affecting them on a microscopic level, cathodoluminescence combined with scanning transmission electron microscopy and spectroscopy was used to measure the luminescence of $In_{0.15}Ga_{0.85}N$ five-period multiquantum wells. The lattice–composition–energy relationship was established with the help of energy-dispersive x-ray spectroscopy, and the bandgaps of $In_{0.15}Ga_{0.85}N$ and GaN in multiple quantum wells were extracted by electron energy loss spectroscopy to understand the features of cathodoluminescence spectra. The luminescence differences between different periods of multiquantum wells and the effects of defects such as composition fluctuation and dislocations on the luminescence of multiple quantum wells were revealed. Our study establishing the direct relationship between the atomic structure of $In_xGa_{1-x}N$ multiquantum wells and photoelectric properties provides useful information for nitride applications.

Keywords: nitride multiquantum wells, defect, cathodoluminescence, scanning transmission electron microscopy

PACS: 85.60.Jb, 62.40.+i, 61.72.–y **DOI:** 10.1088/1674-1056/ad1c56

1. Introduction

III-nitrides (i.e., group VA-III nitrides including InN, GaN and AlN) are widely used in optoelectronic devices because of their large bandgaps, high thermal conductivities, high electron mobilities, and high breakdown field strengths.[1–4] Among them, the light-emitting diodes (LEDs) prepared using multiple quantum wells (MQWs) are environmentally friendly, have a higher energy efficiency than traditional lighting,[5,6] and are widely used in lighting devices.[7] InGaN-based blue LEDs utilize GaN quantum barriers (QBs) between quantum wells (QWs) to limit the carriers, vastly increasing the light efficiency.[8] However, their performance is still limited by problems such as the quantum efficiency decrease.[9–11] One of the primary factors contributing to the decrease in luminescence efficiency is the presence of a piezoelectric polarization field, which was proposed to be induced by stress during epitaxial and doping process on MQWs luminescence.[12,13] Nevertheless, further investigation is required to explore the correlation between microstructure and luminescent properties at the nanoscale for MQWs. Therefore, in order to gain further insights into the luminescence mechanism of MQWs, it becomes imperative to investigate how differences in stress, elemental components and defects among different period QWs influence the luminescent behavior under higher spatial resolution.

In recent years, more in-depth research on the luminescence mechanisms of MQWs has brought luminescence studies to the nanometer scale,[14–18] all of which have been enabled by the development of scanning transmission electron microscopy (STEM)-cathodoluminescence (CL). CL is the ultraviolet, visible, and near-infrared light emitted by materials under the excitation caused by the incidence of high-energy electron beams. The luminescence mechanisms can be divided into incoherent and coherent emissions. The material system that we studied is a direct-bandgap semiconductor in which incoherent emission predominates. In terms of the yield of incoherent emissions, the smaller the voltage, the larger the volume of interactions between the electrons and the mate-

†Corresponding author. E-mail: zhurui@pku.edu.cn
‡Corresponding author. E-mail: tbwei@semi.ac.cn
§Corresponding author. E-mail: xdbai@iphy.ac.cn
¶Corresponding author. E-mail: pgao@pku.edu.cn

© 2024 Chinese Physical Society and IOP Publishing Ltd

rial, and the better the yield. Therefore, an 80 kV voltage was adopted to ensure not only a high output but also a high spatial resolution. On the one hand, compared with other spectral characterization techniques, such as laser-excited photoluminescence (PL),[19,20] CL has several advantages. For example, the source in CL is super-continuous and has a large energy range; hence, CL is suitable for multiple transitions, including broad bandgap transitions and core-level transitions.[21] On the other hand, compared to SEM-CL,[22,23] STEM-CL provides higher spatial resolution and can be combined with high-angle annular dark field (HAADF) image and electron energy loss spectrum (EELS), which can study the optical properties of materials, such as local bandgap changes and defects with nanometer resolution. Therefore, STEM-CL is a powerful method for studying the optoelectrical properties of nanostructures with quantum-size effects in semiconductor optoelectronic devices such as LEDs. Furthermore, there have been several STEM-CL studies that investigated the luminescence of MQWs, encompassing variations in doping condition and thickness among MQWs that lead to distinct luminescent properties.[14,24] However, the effects of discrepancies among different period QWs and defects on the optoelectronic performance of MQWs are still largely unknown.

In this study, we performed STEM-CL to characterize the luminescence of five-period $In_xGa_{1-x}N$/GaN MQWs. Three CL luminescence peaks, including yellow band luminescence (YL), GaN, and MQWs, were observed in the CL spectra; however, the wavelength and intensity of the luminescence could be affected by many universal defects at the nanoscale. Firstly, the piezoelectric polarization fields caused by the strain in different periods of the quantum well led to a change in the luminescence wavelength. The differences in electron and hole mobility can also influence the luminescence intensity. Secondly, in regions with low indium content, the luminescence intensity of CL weakens or even annihilates due to the hindered recombination of electron–hole pairs. Thirdly, the reduced indium content leads to a blue shift in the luminescence spectrum. Finally, owing to the release of strain at the dislocation, the nonradiative recombination rate increases, resulting in a decrease in the luminescence intensity. Our study clarifies the microscopic mechanism for failure analysis of MQW-based devices, creating new tunable factors for the design of new optoelectronic devices.

2. Results and discussion

The five-period $In_xGa_{1-x}N$/GaN MQWs are grown by the metal–organic chemical vapor deposition (MOCVD) method on graphene (Gr)/SiO_2/Si(100) substrates, whose structure is shown in Figs. 1(a) and S1a-b. Our low-temperature STEM-CL system is shown in Fig. 1(b), in which the temperature can be lowered down to 102 K. The two parabolic mirrors and low-temperature environment significantly improve the signal-to-noise ratio (SNR), enabling better CL collection efficiency. However, obtaining high-quality $In_xGa_{1-x}N$ MQWs emission spectra is very challenging at room temperature as the SNR of CL data is poor. On the other hand, although the temperature can be achieved around 102 K, it fails to stabilize at other temperatures for now, making it arduous to compare the cathodoluminescence of MQWs under different thermal conditions. Furthermore, the transmission electrons enable energy-dispersive x-ray spectroscopy (EDS) and EELS measurements in the same area, as shown in Fig. 1(c). The atomic content of In and Ga in the wells is found to be 0.15 and 0.85 by EDS, respectively. According to Vegard's law,[25] the band gap of $In_{0.15}Ga_{0.85}N$ is estimated to be 2.75 eV, and the LED emission wavelength is approximately 450 nm. The EELS mapping to characterize bandgaps of $In_xGa_{1-x}N$ MQWs region is shown in Fig. 1(c), and the typical EELS spectra integrated from the QW and QB are shown in Fig. 1(d), where the bandgaps are extracted by a linear fitting method. The bandgap at InGaN QW is $\sim$ 2.8 eV ($\sim$ 443 nm) and the bandgap at GaN QB is $\sim$ 3.1 eV ($\sim$ 400 nm). The STEM-CL spectrum of $In_xGa_{1-x}N$ MQWs is shown in Fig. 1(e), which exhibits three distinct peaks. The band diagrams of these peaks are shown in Fig. 2(a). Combined with the EELS characterization, the first peak at $\sim$ 400 nm originates from the near-band-edge (NBE) emission of the GaN QBs. The bandgap of the GaN QBs differs from that of bulk GaN ($E_{g,GaN} = 3.4$ eV). This discrepancy arises due to two factors, i.e., the presence of a small amount of indium in GaN QBs and the effects of quantum confinement and Cerenkov loss. The peak at $\sim$ 450 nm is consistent with the front bandgap estimation, which is the NBE luminescence peak of the $In_{0.15}Ga_{0.85}N$ QWs. The last peak at $\sim$ 580 nm originates from the YL owing to the defect state.[26]

To further study the luminescence of each period QW at the microscopic level, we conduct line-scanning STEM-CL experiments with a step length of 1 nm and a probe size of $\sim$ 0.2 nm (Fig. 2(b)). The CL spectral lines of each QW are superimposed in terms of the luminescence wavelength, as shown in Fig. 2(c). The NBE luminescence peak of $In_xGa_{1-x}N$ first exhibits a blue shift, followed by a red shift of $\sim$ 20 nm. The traditional Crosslight APSYS simulation fails to explain this owing to the lack of nonuniform trains in actual MQWs. As shown in Fig. 2(d), owing to the spontaneous polarization of bulk GaN and piezoelectrically induced polarization from the mixing of In element, the combination of the built-in electric field causes energy band bending and electron and hole wave-function separation; this results in the reduction of recombination efficiency and a red shift of the emission wavelength called the quantum-confined Stark effect (QCSE).[27–29] In the structure of the MQWs, the strains in

the periods of the MQWs are not the same. From Figs. 2(e) and S1c-e, the strains in different periods are obtained by geometric phase analysis (GPA),[30–32] which show that the tensile strain decreases in the first two periods and then increases as the QW approached p-GaN. This indicates that the piezoelectrically induced polarization electric field also decreases and increases, resulting in the blue/red shift of the luminescence peak,[33,34] which subsequently leads to the NBE luminescence wavelength undergoing a blue shift followed by a red shift across different periods.

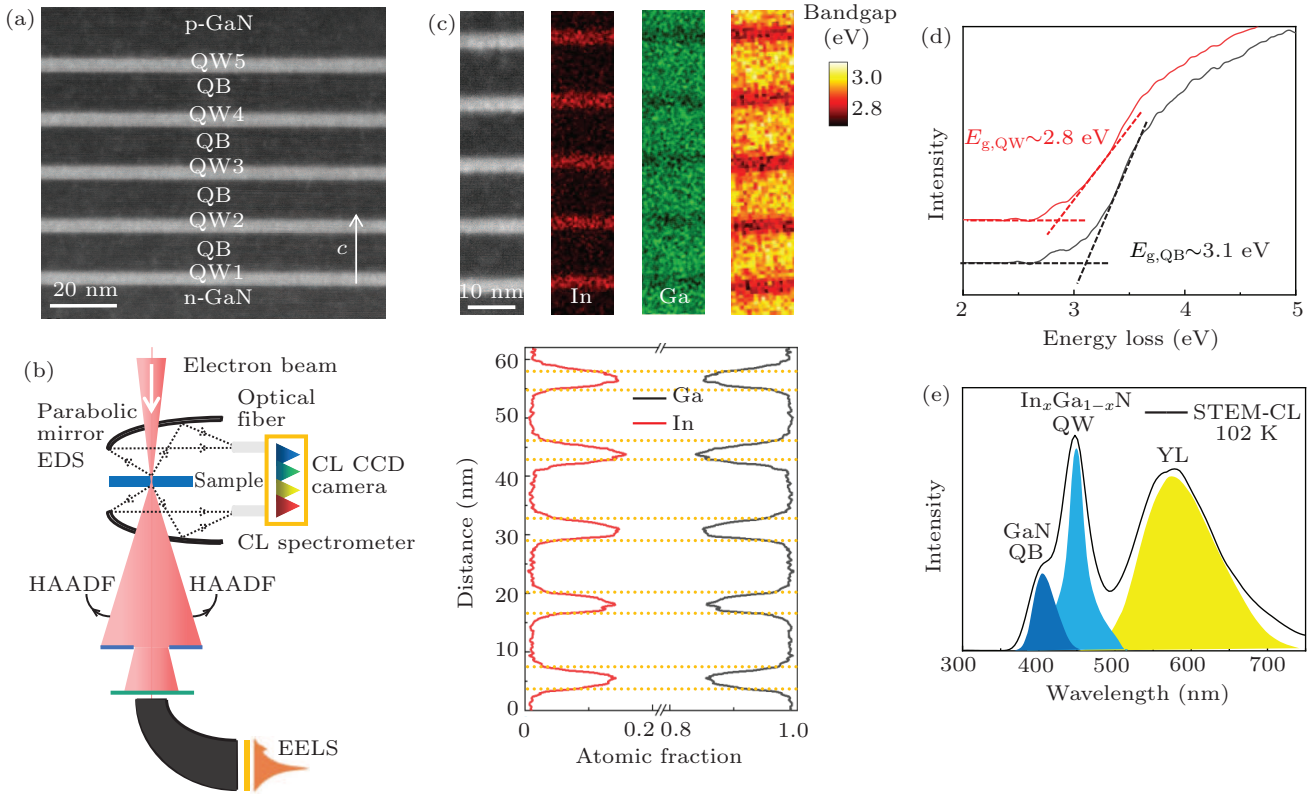


Fig. 1. STEM-CL characterization combined with the HAADF, EDS, and EELS of $In_xGa_{1-x}N$ MQWs. (a) HAADF image of $In_xGa_{1-x}N$ LED. (b) Schematic diagram of STEM-CL, HAADF, EDS and EELS. (c) HAADF image, EDS mappings of In (red), Ga (green), EELS bandgap mapping and atomic fractions of In and Ga of the $In_xGa_{1-x}N$ MQWs. (d) EELS spectrum of QB and QW. (e) STEM-CL spectrum of the $In_xGa_{1-x}N$ MQWs.

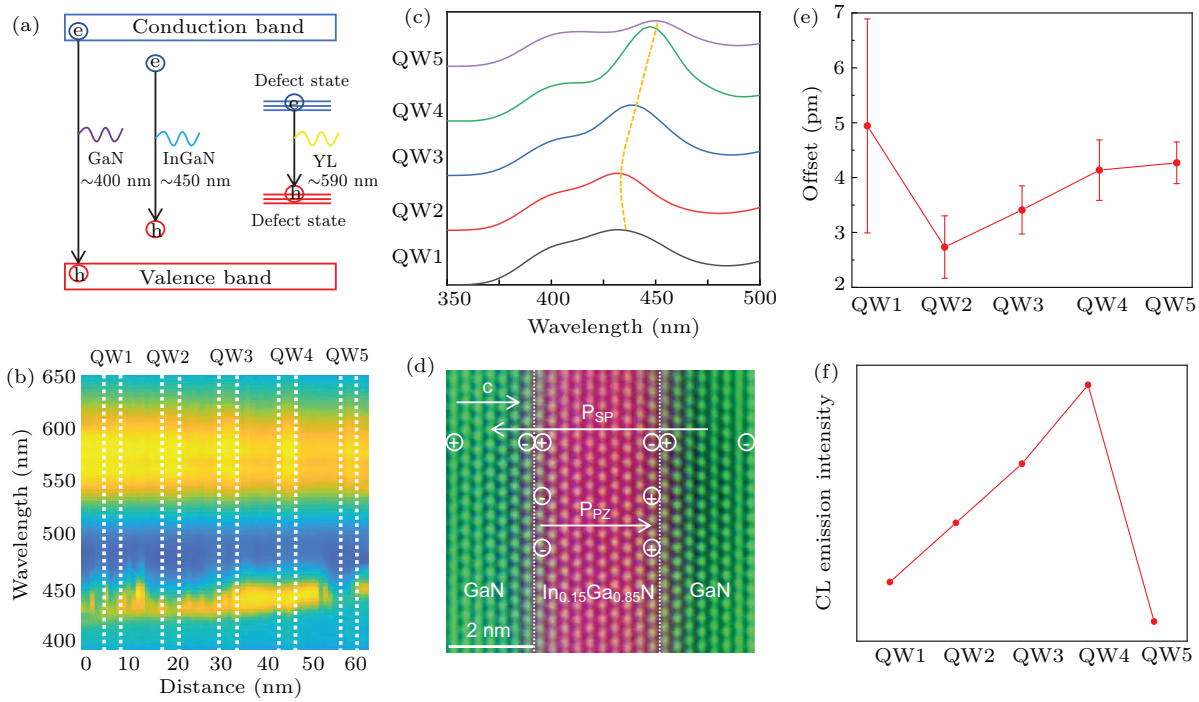


Fig. 2. CL emission difference of five periods of MQWs. (a) Band diagram of three CL emission peaks. (b) STEM-CL mapping across different five periods of MQWs. (c) The shift of NBE wavelength in QWs. (d) Schematic diagram of built-in electric field in MQWs. (e) Line profile of the strain calculated by GPA in QW1–5. (f) Line profile of CL emission intensity in QW1–5.

We also observe that the 4th QW exhibits the strongest light-emitting tendency (Fig. 2(f)). Because the electron mobility is fast and the hole mobility is slow.[35] The electrons and holes recombine mostly in the QW near the p-type GaN, where the luminescence is stronger. However, due to the difference in growth temperature between the final QW and the electron barrier layer, a minor precipitation of indium element occurs as indicated by the EDS measurement (Fig. 1(c)), thereby impacting the growth quality and resulting in the decline of CL luminescence intensity within the last QW.

It is worth noting that there is usually a non-uniform composition in the MQWs. A typical QW with partially missing In is shown in Figs. 3(a) and 3(b), and the atomic fraction change of the In content is shown in Fig. 3(c). We perform a STEM-CL characterization in this region (Fig. 3(d)) and discover that the NBE emission peak of the QW decreases with the composition of In (Fig. 3(e)). Moreover, the CL luminescence intensity weakens or even disappears in the In-deficient region (Fig. 3(f)). This can be explained from the perspective of recombination. According to the different methods of energy release, recombination can be divided into radiation and non-radiation recombination. Direct radiation recombination, which is the primary form of radiation recombination, refers to the process of direct recombination between conduction-band electrons and valence-band holes. It can also be carried out through the recombination center to release energy in other ways, which is called non-radiative recombination. Because the CL can only collect signals of radiation recombination, the reduction of In content makes it difficult to achieve the electron–hole pair recombination, thus enhancing the non-radiative recombination, which weakens the intensity of the CL luminescence.

Additionally, various defects in GaN can affect the luminescence of the MQWs. A HAADF image of a threading dislocation (TD) in the MQWs is shown in Fig. 4(a), which is judged to be a mixed-type dislocation. Previous studies have found it hard to explain the structure–activity relationship between the dislocation and luminescence of MQWs owing to the limitation of spatial resolution.[36–39]

As shown in Fig. 4(b), we study the luminescence of the mixed dislocation region in the MQWs. The NBE luminescence peak of $In_xGa_{1-x}N$ QW around the dislocation has a blue shift of $\sim$ 15 nm (Fig. 4(c)). As Fig. 4(b) shows, the strain is released at the dislocation, and the strain-induced polarization electric field is depressed, which leads to a blue shift of the luminescence peak near the dislocation. On the other hand, Fig. 4(e) shows that the luminescence intensity at the mixed dislocations is significantly weakened, which can be attributed to recombination. As shown in Fig. 4(f), the mixed-type dislocation in n-type GaN is an electron trap with a negative charge, which has a scattering effect on the carriers. The energy generated by the electron and hole recombination is likely to be captured by another electron, resulting in Auger recombination and the formation of a nonradiative recombination center.[40–42] The nonradiative recombination rate thus increases near the dislocation, leading to a decrease in minority carriers and luminescence intensity.

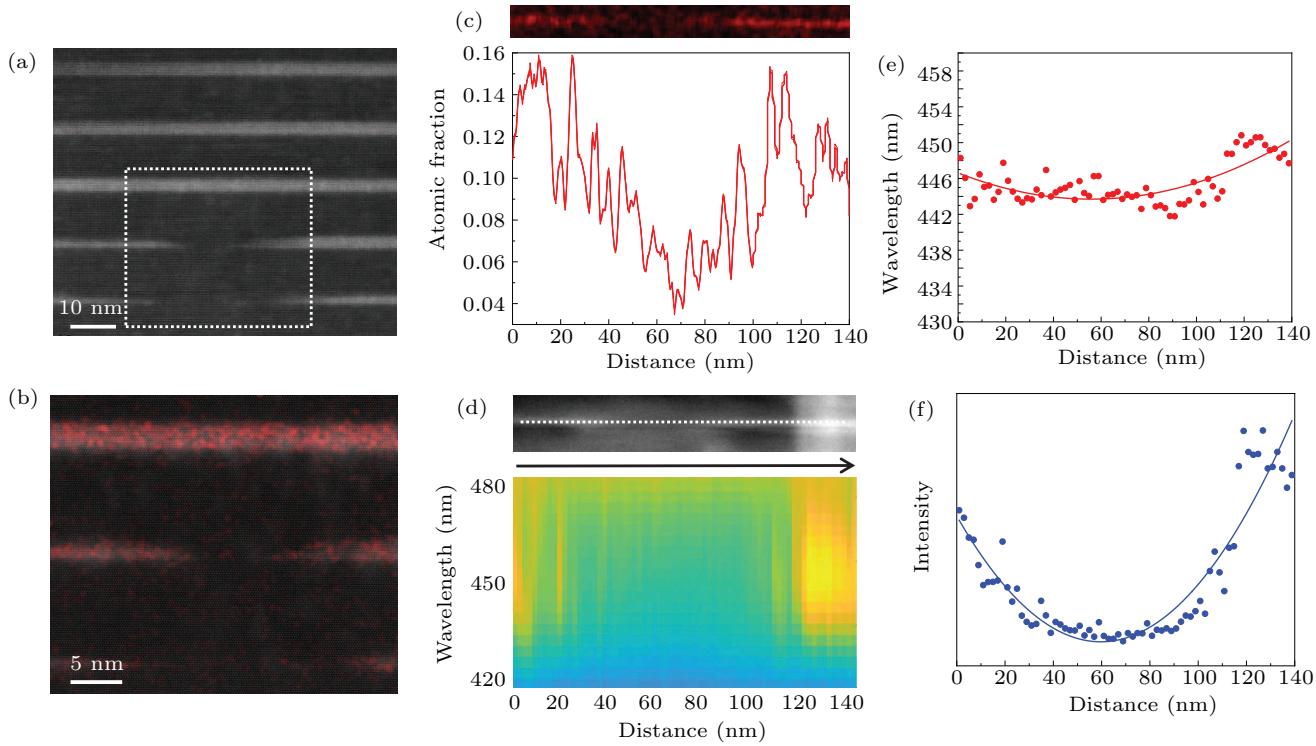


Fig. 3. Effect of In composition fluctuation on CL emission. (a), (b) HAADF image and EDS mapping of local In composition fluctuation in MQWs. (c) Atomic fraction of In element in QW1. (d) STEM-CL mapping across In composition fluctuation region in QW1. (e), (f) Line profile of wavelength and intensity of NBE emission across In composition fluctuation region in QW1.

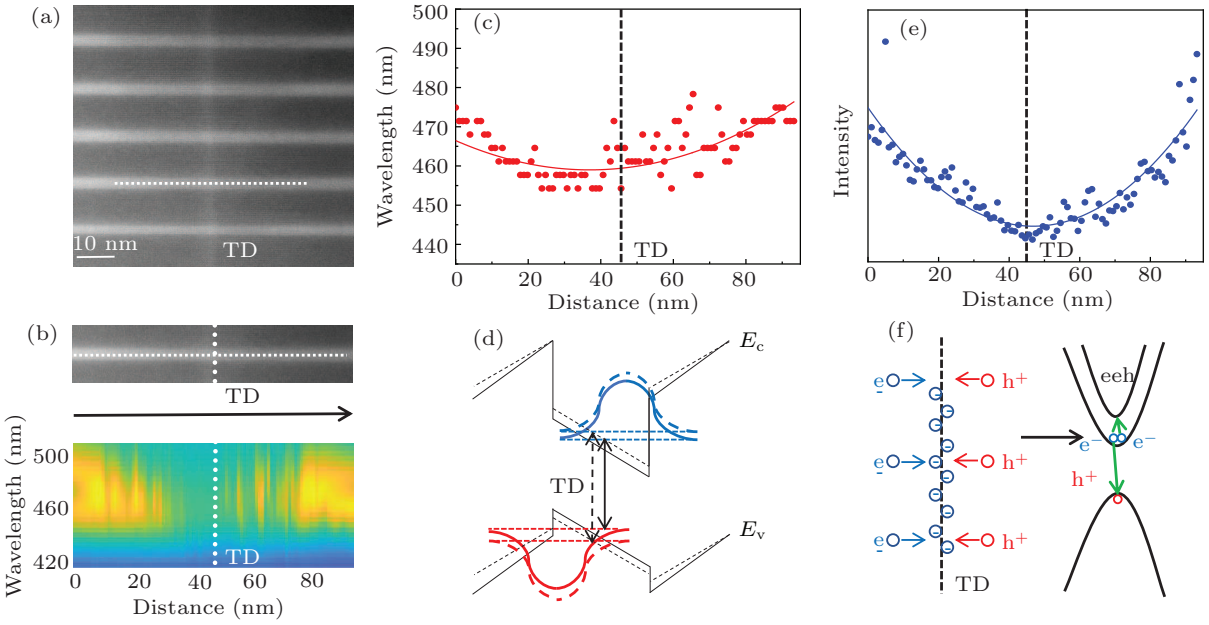


Fig. 4. Effect of the TD on CL emission. (a), (b) HAADF image and STEM-CL mapping of TD in MQWs. (c) Line profile of wavelength of NBE emission across the TD. (d) Schematic diagram showing the effects of the TD on the built-in electric field. (e) Line profile of intensity of NBE emission across the TD. (f) Schematic diagram of the non-radiative recombination mechanism around the TD.

3. Conclusions

Using STEM-CL characterizations at 102 K, we studied the luminescence behavior of five periods of $In_{0.15}Ga_{0.85}N$/GaN MQWs and the influence of defects (including component undulations and dislocations) on luminescence. We found that the strain and defects of the material would affect the recombination process and piezoelectrically-induced polarization electric field, leading to changes in the wavelength and intensity of the MQWs luminescence. Thus, the direct relationship between the atomic structure of $In_xGa_{1-x}N$ MQWs and photoelectric properties was established. These microscopic variations significantly impact the overall performance of the device, necessitating their consideration during both MQWs fabrication and device design.

Appendix A: Methods

A1. MOCVD process of the GaN and blue LED on Gr/SiO_2/Si(100) substrate

Trimethylgallium (TMGa), trimethylaluminum (TMAl), and NH_3 were used as Ga, Al, and N precursors for growing AlN and GaN films. The III-nitride films were grown on the Gr/SiO_2/Si(100) substrate using the Veeco K300 MOCVD chamber. First, the high temperature (HT)-AlN was grown at 1200 °C for 6 min with the NH_3 flow of 1000 sccm and TMAl flow of 50 sccm. Then the 1st-GaN layer was grown at 1050 °C for 40 min. After that 5 periods of $In_xGa_{1-x}N$/GaN MQWs layer were grown at 735 °C/834 °C with 3 nm InGaN well layers and 12 nm GaN barriers. The active layers were capped with a p-GaN layer deposited at 950 °C with the biscyclopentadienyl magnesium (Cp2Mg) flow of 120 sccm, followed by an annealing process at 720 °C for 10 min under N_2 ambient.

A2. Electron microscopy characterizations and analysis

The cross-sectional TEM specimen was made by the ThermoFisher Helios G4 UX focused ion beam system. The HAADF and EDS mapping were performed using FEI Titan Cubed Themis G2 300 spherical aberration corrected STEM, operated at 300 kV. The convergence semi angle was 30 mrad and the collection semi angle of HAADF was 39–200 mrad. The camera length in HAADF mode was set as 145 mm. The STEM-CL spectra were taken on JEOL Grand ARM 300 equipped with a Vulcan CL detector, operated at 80 kV.

Acknowledgements

Projct supported by the National Key R&D Program of China (Grant No. 2019YFA0708202), the National Natural Science Foundation of China (Grant Nos. 11974023, 52021006, 61974139, 12074369, and 12104017), the "2011 Program" from the Peking–Tsinghua–IOP Collaborative Innovation Center of Quantum Matter, and the Youth Supporting Program of Institute of Semiconductors. We acknowledge Electron Microscopy Laboratory of Peking University and Institute of Physics of Chinese Academy of Sciences for the use of electron microscopes.

References

[1] Ponce F A and Bour D P 1997 *Nature* **386** 351
[2] Pimputkar S, Speck J S, DenBaars S P and Nakamura S 2009 *Nat. Photonics* **3** 179
[3] Kobayashi Y, Kumakura K, Akasaka T and Makimoto T 2012 *Nature* **484** 223
[4] Guo L, Guo Y, Wang J and Wei T 2021 *Journal of Semiconductors* **42** 081801

[5] Humphreys C J 2008 *MRS Bull.* **33** 459
[6] Schubert E F and Kim J K 2005 *Science* **308** 1274
[7] Sheu J K, Chang S J, Kuo C H, Su Y K, Wu L W, Lin Y C, Lai W C, Tsai J M, Chi G C and Wu R K 2003 *IEEE Photonics Technol. Lett.* **15** 18
[8] Kuo Y, Chang J, Tsai M and Yen S 2009 *Appl. Phys. Lett.* **95** 011116
[9] Rozhansky I V and Zakheim D A 2007 *Phys. Stat. Sol. (a)* **204** 227
[10] Kim M H, Schubert M F, Dai Q, Kim J K, Schubert E F, Piprek J and Park Y 2007 *Appl. Phys. Lett.* **91** 183507
[11] Schubert M F, Xu J, Kim J K, Schubert E F, Kim M H, Yoon S, Lee S M, Sone C, Sakong T and Park Y 2008 *Appl. Phys. Lett.* **93** 041102
[12] Liu M, Yang Y, Xiang P, Chen W, Han X, Lin X, Lin J, Luo H, Liao Q, Zang W, Wu Z, Liu Y and Zhang B 2015 *Chin. Phys. B* **24** 068503
[13] Wael Z T, Gil Y H, Sang W R, June S H and June K L 2016 *Optical Materials* **55** 17
[14] James T G, Zhang S, Bertrand R, Fu W, Bao A, Zhu D, David J, Ashley H, Ian B, David S, Menno J, Colin J H and Rachel A O 2015 *Nano Lett.* **15** 7639
[15] Sung K L, Megan B, Qian F, Li Y, Charles M L and Silvija G 2009 *Nano Lett.* **9** 3940
[16] Peter S, Shawn W and Eli S 2019 *Nature* **570** 354
[17] Michal, V, Daniel K A, Fariah H, Katherine S and Jennifer A D 2018 *Nat. Commun.* **9** 4658
[18] Sheng B, Schmidt G, Bertram F, Veit P, Wang Y, Wang T, Rong X, Chen Z, Wang P, Bläsing J, Miyake H, Li H, Guo S, Qin Z, Strittmatter A, Shen B, Christen J and Wang X 2020 *Photonics Research* **8** 610
[19] Deguchi T, Shikanai A, Torii K, Sota T, Chichibu S and Nakamura S 1998 *Appl. Phys. Lett.* **72** 3329
[20] Cho Y H, Song J J, Keller S, Minsky M S, Hu E, Mishra U K and DenBaars S P 1998 *Appl. Phys. Lett.* **73** 1128
[21] Rothwarf A 1973 *J. Appl. Phys.* **44** 752
[22] Merano M, Sonderegger S, Crottini A, Collin S, Renucci P, Pelucchi E, Malko A, Baier M H, Kapon E, Deveaud B and Ganiere J D 2005 *Nature* **438** 479
[23] Sonderegger S, Feltin E, Merano M, Crottini A, Carlin J F, Sachot R, Deveaud B, Grandjean N and Ganiere J D 2006 *Appl. Phys. Lett.* **89** 232109
[24] Marcus M, Gordon S, Sebastian M, Peter V, Frank B, Robert A R L, Dominik H, Wang J, Tobias M, Ferdinand S and Jurgen C 1999 *Phys. Status Solidi B* **253** 112
[25] Kuo Y, Liou B, Yen S and Chu H 2004 *Opt. Commun.* **237** 363
[26] Egerton R F 2009 *Rep. Prog. Phys.* **72** 016502
[27] Miller D, Chemla D, Damen T, Gossard A, Wiegmann W, Wood T and Burrus C 1984 *Phys. Rev. Lett.* **53** 2173
[28] Fiorentini V, Bernardini F, Della S F, Di Carlo A and Lugli P 1999 *Phys. Rev. B* **60** 8849
[29] Tetsuya T, Shigetoshi S, Hiromitsu S, Hiroshi A, Isamu A, Yawara K, Shigeru N, Yishifumi Y, Norihide Y 1998 *Journal of Crystal Growth* **189** 616
[30] RouviereJ L and Sarigiannidou E 2005 *Ultramicroscopy* **106** 1
[31] Zhao C W, Xing Y M, Bai P C, Hou J F and Dai X J 2008 *Physica B* **403** 1838
[32] Jayhoon C and Lew R 2008 *Ultramicroscopy* **108** 1595
[33] Anna R, Aleksandra W, Kamil S, Uwe J, Ute Z, Andrian V K, Agnieszka P, Marta S, Kamil K, Zbigniew R Z and Bogdan J K 2016 *J. Appl. Phys.* **120** 194304
[34] Xue H, Pan N, Li M, Wu Y, Wang X and Hou J 2010 *Nanotechnology* **21** 215701
[35] Zhang J, Cai L, Zhang B, Hu X, Jiang F, Yu J and Wang Q 2009 *Appl. Phys. Lett.* **95** 161110
[36] Speck J S and Rosner S J 1999 *Physica B* **273** 24
[37] Yacobi B G and Holt D B 1986 *J. Appl. Phys.* **59** R1
[38] Agata B, Łucja M, Julita S, Szymon G, Jan W, Dario S and Piotr P 2021 *Scientifc Reports* **11** 21
[39] Barbara B, Frank B, Juergen C, Thomas H, Armin D and Alois K 2009 *Appl. Phys. Lett.* **95** 032106
[40] ShenY C, Mueller G O, Watanabe S, Gardner N F, Munkholm A and Krames M R 2007 *Appl. Phys. Lett.* **91** 141101
[41] Mukai T, Yamada M and Nakamura S 1999 *Jpn. J. Appl. Phys.* **38** 3976
[42] Albrecht M, Weyher J L, Lucznik B, Grzegory I and Porowski S 2008 *Appl. Phys. Lett.* **92** 231909